Available online at www.sciencedirect.com
SCIENCE DIRECT®
International Journal of Heat and Fluid Flow 26 (2005) 810–816
International Journal of HEAT AND FLUID FLOW
www.elsevier.com/locate/ijhff

A computational study of natural convection in a liquid-encapsulated molten semiconductor with a horizontal magnetic field

Mei Yang, Nancy Ma *

Department of Mechanical and Aerospace Engineering, North Carolina State University, Campus Box 7910, Raleigh NC 27695, USA

Received 11 December 2004; accepted 28 March 2005
Available online 2 June 2005

Abstract

This paper treats the natural convection in a layer of boron oxide, called a liquid encapsulant, which lies above a layer of a molten compound semiconductor (melt) between cold and hot vertical walls in a rectangular container with a steady horizontal magnetic field B. The magnetic field provides an electromagnetic (EM) damping of the molten semiconductor which is an excellent electrical conductor but has no direct effect on the motion of the liquid encapsulant. This study uses a Chebyshev spectral collocation method to investigate the coupling between the natural convection in the boron oxide and melt.

Keywords: Semiconductor crystal growth; Magnetic fields; III–V Compounds; Computational model

1. Introduction

The physical understanding of flows that occur during melt growth of semiconductor crystals is key to the development of optimal electromagnetic crystal growth systems. Since molten semiconductors are excellent electrical conductors, the melt motion can be damped and controlled by a steady (DC) magnetic field in order to control the species distribution in the crystal, which depends on the convective and diffusive transport of the species in the melt. Electronic and optical devices are manufactured on single-crystal wafers sliced from ingots of semiconductor crystals. Since the performance of any device depends strongly on the uniformity of the local concentration in the wafer on which it is produced, a major objective during the solidification of any semiconductor is to minimize segregation in the crystal.

During the magnetic liquid encapsulated Czochralski (MLEC) growth of compound semiconductor crystals, such as indium-phosphide (InP), phosphorus gas is bubbled at high pressure through an indium melt, and the indium and phosphorus fuse to form the compound InP. A layer of boron oxide (B_2O_3) encapsulates the melt to prevent escape of the volatile component (P). A single-crystal seed is lowered through the encapsulant which initiates solidification and crystal growth begins in the presence of an externally applied magnetic field. Morton et al. (2002) presented a model of dopant transport during the MLEC process. Previous researchers have investigated the effect of a steady magnetic field on two-dimensional natural convection in rectangular enclosures (Ozoe and Okada, 1989; Burr and Müller, 2001; Mossner and Muller, 1999; Di Piazza and Ciofalo, 2002; Authie et al., 2003; Garandet et al., 1992; Alchaar et al., 1995). Previous research which has treated systems that have liquid encapsulation have neglected any coupling between the natural convections in the molten semiconductor and in the liquid encapsulant and

* Corresponding author. Tel.: +1 919 515 5231; fax: +1 919 515 7968.
E-mail address: nancy_ma@ncsu.edu (N. Ma).

0142-727X/$ - see front matter © 2005 Elsevier Inc. All rights reserved.
doi:10.1016/j.ijheatfluidflow.2005.03.010

assumed that the liquid encapsulant is stagnant (Ma et al., 1998; Ma and Walker, 1995). Recently, Kuniholm and Ma (2003) used an asymptotic analysis in order to investigate the interaction between the melt and the encapsulant in a rectangular enclosure with strong magnetic fields. Series and Hurle (1991) and Walker (1999) have reviewed the use of magnetic fields during semiconductor crystal growth.

Recent experiments (Riemann et al., 1996) have shown some very promising results with a steady horizontal magnetic field, which is obtained by placing the crystal-growth furnace between the pole faces of an iron-yoke magnet. Williams and Walker (1990) have investigated the effects of a horizontal magnetic field on melt motion during Czochralski crystal growth. Previously, we treated the simplified asymptotic equations which are valid for a strong magnetic field for which $Ha \gg 1$ (Kuniholm and Ma, 2003). Here, the Hartmann number is $Ha = BL(\sigma/\mu)^{1/2}$, where B is the magnetic flux density and L is the width of the molten semiconductor (melt) or liquid encapsulant while σ and μ are the melt's electrical conductivity and dynamic viscosity, respectively. We investigated the coupling between the natural convection in the liquid encapsulant and in the molten semiconductor in a rectangular enclosure with a strong horizontal magnetic field. For a strong magnetic field, we were justified in neglecting effects of inertia and convective heat transfer (Ma and Walker, 2001). In an asymptotic solution for the inertialess convectionless melt motion for $Ha \gg 1$, the melt is divided into (i) an inviscid core region, (ii) Hartmann layers with an $O(Ha^{-1})$ thickness carrying an $O(Ha^{-1})$ flow adjacent to the hot and cold walls, and (iii) parallel layers with an $O(Ha^{-1/2})$ thickness carrying an $O(Ha^{1/2})$ flow adjacent to the bottom wall and adjacent to the encapsulant–melt interface. The Hartmann layers have a simple, local, exponential structure, match any vertical core or parallel layer velocities, and satisfy the boundary conditions along the hot and cold walls. We consistently neglected an $O(Ha^{-1})$ perturbation, neglected the Hartmann layers and relaxed the no-slip conditions along the core adjacent to the hot and cold walls.

In the present study, we investigate the natural convection in the same configuration as Kuniholm and Ma (2003). The configuration treated here is a very simplified model for two-dimensional flow in a rectangular enclosure. The flow would be very different for a three-dimensional configuration. The purpose of the present study is to develop a computational method and to understand the basic physics in a simplified problem. However, this investigation is very different from our previous asymptotic treatment because we use a numerical approach to treat the full equations in the entire volume of the melt so that our solution is valid for any value of the magnetic field strength.

2. Problem formulation

This paper treats the two-dimensional natural convection in two layers of fluid with a molten semiconductor (melt) encapsulated by a layer of boron oxide in a steady horizontal or transverse magnetic field $\mathbf{B}\hat{\mathbf{x}}$. Here, B is the magnetic flux density while $\hat{\mathbf{x}}$ and $\hat{\mathbf{y}}$ are the unit vectors for the Cartesian coordinate system. Our dimensionless problem is sketched in Fig. 1. The coordinates and lengths are normalized by the length of the melt or boron oxide L, so that α and $(\gamma - \alpha)$ are the dimensionless depths of the melt and boron oxide, respectively. Along $x = 0$ and $x = 1$, the liquids are maintained at temperatures T_c and T_h, respectively, where $T_h > T_c$. The boundaries at $y = 0$ and $y = \gamma$ are thermal insulators. Here, the fluid flows are driven by the temperature difference so that the characteristic velocities for the natural convection in the melt (Hjellming and Walker, 1987) and in the encapsulant are

$$U = \frac{\rho g \beta (\Delta T)}{\sigma B^2}, \quad U_e = \frac{\rho_e g \beta_e (\Delta T) L^2}{\mu_e}, \tag{1a, 1b}$$

respectively, where $(\Delta T) = T_h - T_c$ is the characteristic temperature difference and g is gravitational acceleration. Here, ρ, β, and σ are the density, thermal volumetric expansion coefficient and electrical conductivity of the melt while ρ_e, β_e, and μ_e are the density, thermal volumetric expansion coefficient and dynamic viscosity of the encapsulant. We use the thermophysical properties of molten indium-phosphide and boron oxide, as shown in Table 1. With $(\Delta T) = 50$ K and $L = 5$ cm (Farrell and Ma, 2002), the characteristic velocity in the encapsulant is $U_e = 0.014065$ m/s while the characteristic velocity in the melt is 0.006284 or 0.00006284 m/s for $B = 0.5$ or 5 T, respectively.

The electric current in the melt produces an induced magnetic field which is superimposed upon the applied magnetic field produced by the external magnet. The characteristic ratio of the induced to applied magnetic field strengths is the magnetic Reynolds number,

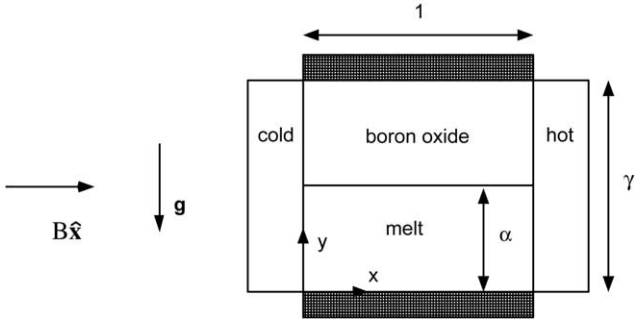

Fig. 1. Two-dimensional problem with a liquid encapsulant and molten semiconductor with a uniform, steady, horizontal magnetic field $B\hat{\mathbf{x}}$ and with coordinates normalized by the distance between the hot and cold vertical walls.

Table 1
Thermophysical properties of molten InP and B_2O_3

Property	Molten InP	B_2O_3
Viscosity (Pa s)	8.19×10^{-4}	10
Density (kg/m^3)	5050	1530
Specific heat (J/kg K)	424	1864.3
Thermal conductivity (W/m K)	22.8	2.0
Thermal volumetric expansion coefficient (K^{-1})	4.44×10^{-4}	7.5×10^{-5}
Electrical conductivity (Ω^{-1} m^{-1})	7×10^5	0.0

$R_m = \mu_p\sigma UL$, where μ_p is the magnetic permeability of the melt. For all crystal-growth processes, $R_m \ll 1$ and the additional magnetic fields produced by the electric currents in the melt are negligible.

Using the Boussinesq approximation, the natural convection in the melt is governed by

$$N^{-1}(\mathbf{v}\cdot\nabla)\mathbf{v} = -\nabla p + T\hat{\mathbf{y}} + \mathbf{j}\times\hat{\mathbf{x}} + Ha^{-2}\nabla^2\mathbf{v}, \tag{2a}$$

$$\nabla\cdot\mathbf{v} = 0, \tag{2b}$$

$$\nabla\cdot\mathbf{j} = 0, \tag{2c}$$

$$\mathbf{j} = -\nabla\phi + \mathbf{v}\times\hat{\mathbf{x}}, \tag{2d}$$

$$Pe_t(\mathbf{v}\cdot\nabla)T = \nabla^2 T, \tag{2e}$$

where $\mathbf{v} = u\hat{\mathbf{x}} + v\hat{\mathbf{y}}$ is the melt's velocity normalized by U, p is the deviation from hydrostatic pressure normalized by $\rho g\beta(\Delta T)L$, $\mathbf{j}$ is the electric current density normalized by σUB, ϕ is the electric potential normalized by UBL, and T is the deviation of the melt's temperature from T_c normalized by (ΔT). Eq. (2a) is the Navier–Stokes equation the interaction parameter $N = \sigma B^2 L/\rho U$ is the characteristic ratio of the electromagnetic (EM) body force term to the inertial terms. Eqs. (2b) and (2c) are conservation of mass and electric current, respectively. Eq. (2d) is Ohm's law for a horizontal magnetic field. Eq. (2e) is the energy equation where the thermal Péclet number $Pe_t = \rho c_p UL/k$ is the characteristic ratio of convective to conductive heat transfer. Here, c_p and k are the melt's specific heat and thermal conductivity, respectively.

For the present plane recirculating flow in the melt, the condition of zero net electric current in the z direction in combination with electrically insulating boundaries implies that the electric field is zero (Hirtz and Ma, 2000). The only non-zero component of the electric current density, normalized by σUB, is given by Ohm's law, $j_z = -v$.

With the Boussinesq approximation, the natural convection in the encapsulant is governed by

$$Re(\mathbf{v}_e\cdot\nabla)\mathbf{v}_e = -\nabla p_e + T_e\hat{\mathbf{y}} + \nabla^2\mathbf{v}_e, \tag{3a}$$

$$\nabla\cdot\mathbf{v}_e = 0, \tag{3b}$$

$$Pe_{te}(\mathbf{v}\cdot\nabla)T_e = \nabla^2 T_e, \tag{3c}$$

where $\mathbf{v}_e = u_e\hat{\mathbf{x}} + v_e\hat{\mathbf{y}}$ is the encapsulant's velocity normalized by U_e, p_e is the deviation of the encapsulant's pressure from the hydrostatic pressure normalized by $\mu_e U_e/L$, and T_e is the deviation of the encapsulant's temperature from T_c normalized by (ΔT). Here, μ_e is the dynamic viscosity of the liquid encapsulant. Eq. (3a) is the Navier–Stokes equation where the Reynolds number $Re = \rho_e U_e L/\mu_e$ is the characteristic ratio of the inertial force to the viscous force in the encapsulant. Here, ρ_e is the encapsulant's density. Eq. (3b) is conservation of mass. Eq. (3c) is the energy equation where the encapsulant's thermal Péclet number $Pe_{te} = \rho_e c_{pe} U_e L/k_e$ is the characteristic ratio of convective to conductive heat transfer in the encapsulant. Here, c_{pe} and k_e are the specific heat and thermal conductivity of the encapsulant, respectively.

We apply the no-slip and no-penetration conditions along the walls at $x = 0$, $x = 1$, $y = 0$ and $y = \gamma$. Along the planar interface, the no-slip and no-penetration conditions (Farrell and Ma, 2002) are

$$u(x,\alpha) = \frac{\lambda_\beta}{\lambda_\mu} Ha^2 u_e(x,\alpha), \quad \text{for} \quad 0 \leqslant x \leqslant 1, \tag{4a}$$

$$v(x,\alpha) = 0, \quad \text{for} \quad 0 \leqslant x \leqslant 1, \tag{4b}$$

$$v_e(x,\alpha) = 0, \quad \text{for} \quad 0 \leqslant x \leqslant 1, \tag{4c}$$

where $\lambda_\beta = \rho_e\beta_e/(\rho\beta)$ and $\lambda_\mu = \mu_e/\mu$. With boron oxide and molten indium-phosphide, $\lambda_\beta = 0.051177$ and $\lambda_\mu = 12210$. The stress is continuous across the interface (Farrell and Ma, 2002) so that

$$\frac{\partial u}{\partial y}(x,\alpha) = \lambda_\beta Ha^2 \frac{\partial u_e}{\partial y}(x,\alpha), \quad \text{for} \quad 0 \leqslant x \leqslant 1. \tag{5}$$

Here, the gradients of the interfacial tension due to gradients of the temperature or of concentration along the encapsulant–melt interface are negligible (Kuniholm and Ma, 2003). A measure of the effects of interfacial tension gradients is the Marangoni number for the encapsulant, $Ma_e = \rho_e(-\mathrm{d}\Gamma/\mathrm{d}T)(\Delta T)L/\mu_e^2$, where Γ is the interfacial tension of the encapsulant–melt interface. There are no published data on the tension of an interface between a liquid semiconductor and boron oxide. If we use the values of Γ for a liquid-silicon free surface, which are certainly much larger than those for an encapsulant–melt interface, we find that $Ma_e = 0.00516$ for our typical process.

The temperatures along $x = 0$ and $x = 1$ are the cold and hot wall temperatures, respectively, while the top and bottom of the container are insulated. The temperature and heat transfer in the melt and in the encapsulant are continuous across $y = \alpha$. Therefore, the thermal boundary conditions are

$$T(0,y) = 0, \quad \text{for} \quad 0 \leqslant y \leqslant \alpha, \tag{6a}$$

$$T_e(0,y) = 0, \quad \text{for} \quad \alpha \leqslant y \leqslant \gamma, \tag{6b}$$

$$T(1,y) = 1, \quad \text{for} \quad 0 \leqslant y \leqslant \alpha, \tag{6c}$$

$$T_e(1,y) = 1, \quad \text{for} \quad \alpha \leqslant y \leqslant \gamma, \tag{6d}$$

$$\frac{\partial T}{\partial y}(x,0)=0, \quad \text{for} \quad 0\leqslant x\leqslant 1. \tag{6e}$$

$$\frac{\partial T_e}{\partial y}(x,\gamma)=0, \quad \text{for} \quad 0\leqslant x\leqslant 1, \tag{6f}$$

$$T(x,\alpha)=T_e(x,\alpha), \quad \text{for} \quad 0\leqslant x\leqslant 1. \tag{6g}$$

$$\frac{\partial T_e}{\partial y}(x,\alpha)=\lambda_k\frac{\partial T_e}{\partial y}(x,\alpha), \quad \text{for} \quad 0\leqslant x\leqslant 1, \tag{6h}$$

where $\lambda_k = k_e/k$. Here, k and k_e are the thermal conductivities of the melt and the encapsulant, respectively. With boron oxide and molten indium-phosphide, $\lambda_k = 0.08772$.

Eqs. (2)–(6) were solved using a Chebyshev spectral collocation method with Gauss-Lobatto collocation points in x and y. Since Eqs. (2a), (2e), (3a), and (3c) are non-linear, we used a Newton–Raphson iterative method. We used rescaled coordinates for our spectral collocation method. Our rescaled horizontal coordinate is $\xi = 2x - 1$ so that $-1 \leqslant \xi \leqslant +1$. In the melt, our rescaled vertical coordinate is $\eta = (2y - \alpha)/\alpha$ so that $-1 \leqslant \eta \leqslant +1$. In the encapsulant, our rescaled vertical coordinate is $\chi = (2y - \gamma - \alpha)/(\gamma - \alpha)$ so that $-1 \leqslant \chi \leqslant +1$. We use a sufficient number of collocation points in order to resolve the velocity and temperature gradients. The number of collocation points in each direction in both the melt and the encapsulant were increased until the results were independent of these numbers. Of course, the required number of collocation points increased as B was increased because the thickness of the boundary layers decreased and the velocity gradients increased. For example, for $B = 1$ T and $\alpha = 0.6$, we used 31 collocation points in the ξ direction, 31 collocation points in the η direction in the melt and 31 collocation points in the χ direction in the encapsulant. When we doubled the number of collocation points in the ξ direction, the maximum value of the streamfunctions in the melt and encapsulant changed by 0.08% and 0.1%, respectively. When we doubled the number of collocation points in the η direction in the melt, the maximum value of the streamfunction in the encapsulant did not change and the maximum value of the streamfunction in the melt changed by only 0.0004%. When we doubled the number of collocation points in the χ direction in the encapsulant, the maximum value of the streamfunctions in the melt and encapsulant did not change.

3. Results

During the liquid-encapsulated Czochralski process, a molten semiconductor (melt) is contained in a crucible which is heated by radio-frequency induction heating. In order to keep the volatile component, i.e. P in InP, from escaping, the melt is encapsulated with liquid boron oxide. A single-crystal seed is lowered to the surface of the melt and initiates solidification. The crystal grows vertically downward into the melt and radially outward. Once the crystal reaches the desired diameter, the crystal is continuously "pulled" vertically upward until the entire melt's volume is solidified. Prior to solidification in the liquid-encapsulated Czochralski process, the axisymmetric melt is entirely encapsulated by the boron oxide. After a single-crystal seed initiates solidification and the crystal is pulled vertically upward, the encapsulant's depth increases and the melt's depth decreases due to solidification. Once the top of the crystal is pulled out of the encapsulant, the encapsulant's depth is constant while the melt's depth continues to decrease. The melt's depth decreases from an initial value of $\alpha = 0.6$ until the melt has disappeared. The purpose of the present paper is to illustrate the degree of coupling for various magnetic field strengths so we only present results for $(\gamma - \alpha) = 0.2666$ and for melt depths corresponding to the beginning of growth for $\alpha = 0.6$. The dimensionless parameters as a function of the magnetic field strength are $Ha = 1461.76B$, $N = 4412.75B^4$, $Pe_t = 7.3750B^{-2}$ and the characteristic velocity of the melt is $U = 0.0015706B^{-2}$, where B is in T and U is in m/s. The characteristic velocity in the encapsulant is $U_e = 0.014065$ m/s.

With the cold and hot walls at the left and right, respectively, the temperature gradient drives counterclockwise circulations in both the melt and the encapsulant. These circulations alone would lead to positive and negative values of u in the encapsulant and in the melt, respectively, near the interface. Therefore the shear stress σ_{xy} along the interface is always positive, i.e., a force to the left along the bottom of the encapsulant and an equal force to the right along the top of the melt. A positive value of u would reflect dominance by the encapsulant's circulation, resulting in a clockwise circulation in the melt near the interface. A negative interfacial u would reflect dominance by the melt circulation, resulting in a clockwise circulation in the encapsulant near the interface. For $B = 5$ T and $B = 1$ T, the interfacial u is positive, which reflects a dominance by the natural convection in the encapsulant. For $B = 0.4$ T, the interfacial u is negative, which reflects a dominance by the natural convection in the melt but this dominance decreases as the field strength is increased.

For $\alpha = 0.6$, which corresponds to an early stage of growth, we present the dimensional interfacial shear stress for various magnetic field strengths in Fig. 2. For $B = 0.4$ T, the natural convection in the melt is relatively strong and produces a relatively large shear stress along the bottom of the encapsulant. As the magnetic field strength is increased, the magnitude of the natural convection in the melt decreases roughly as B^{-2}, as reflected by our choice for the characteristic velocity in Eq. (1a). The effect of the electromagnetic damping is reflected in the dramatic decrease of the maximum magnitude of the melt's velocity for $\alpha = 0.6$ which is

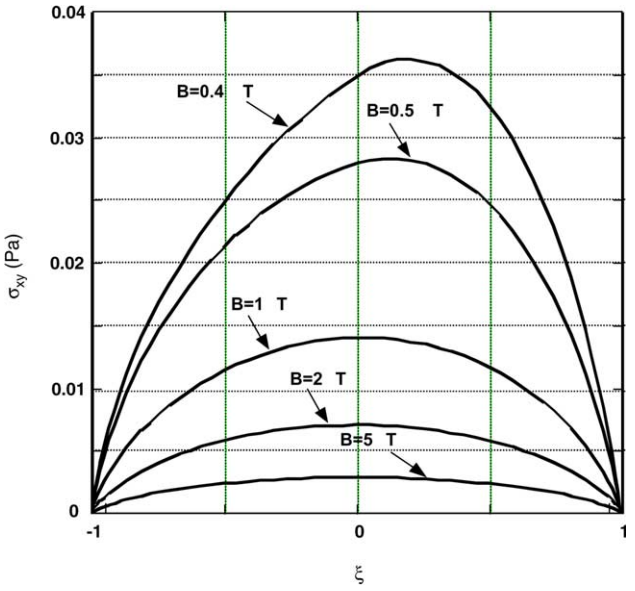

Fig. 2. Interfacial shear stress σ_{xy} versus ξ with $\alpha = 0.6$ for $B = 0.4$, 0.5, 1, 2 and 5 T.

0.02359 m/s for $B = 0.4$ T and 0.0005303 m/s for $B = 5$ T.

For $\alpha = 0.6$ and $B = 5$ T, we present the isotherms and streamlines in the melt in Fig. 3a and b, respectively. For this value of B, the dimensionless parameters are $Ha = 7308.8$, $N = 2.75797 \times 10^6$ and $Pe_t = 0.294998$, and the characteristic velocity in the melt is $U = 0.000062824$ m/s. The isotherms in Fig. 3a are vertical which reflect that the heat transfer is dominated by conduction. In the melt, the hot fluid rises adjacent to $\xi = +1$, flows to the left along the encapsulant–melt interface, sinks adjacent to $\xi = -1$, and flows to the right along the bottom. For this strong field, there is a significant EM damping of the melt motion so that the maximum magnitude of the melt's dimensional velocity is 0.0005303 m/s. The maximum magnitude of the encapsulant's dimensional velocity is 4.7007×10^{-6} m/s. In Fig. 3b, the maximum value of the streamfunction is 0.12983. In an inertialess convectionless asymptotic treatment for $Ha \gg 1$, $O(Ha^{-1/2})$ parallel layers adjacent to $\eta = \pm 1$ carry an $O(Ha^{1/2})$ flow. While the present solution is a numerical solution for the full equations, there is still a large flow adjacent to $\eta = \pm 1$, which is reflected in the crowding of the streamlines adjacent to $\eta = \pm 1$ in Fig. 3b. We present the isotherms and streamlines in the encapsulant in Fig. 4a and b, respectively. The isotherms in Fig. 4a are vertical which reflect that the heat transfer is dominated by conduction. In Fig. 4b, the encapsulant's circulation is counterclockwise with a positive interfacial velocity and the maximum value of the encapsulant's streamfunction is 0.000024928. The natural convection in the encapsulant dominates and drives a positive interfacial velocity in the melt and a clockwise

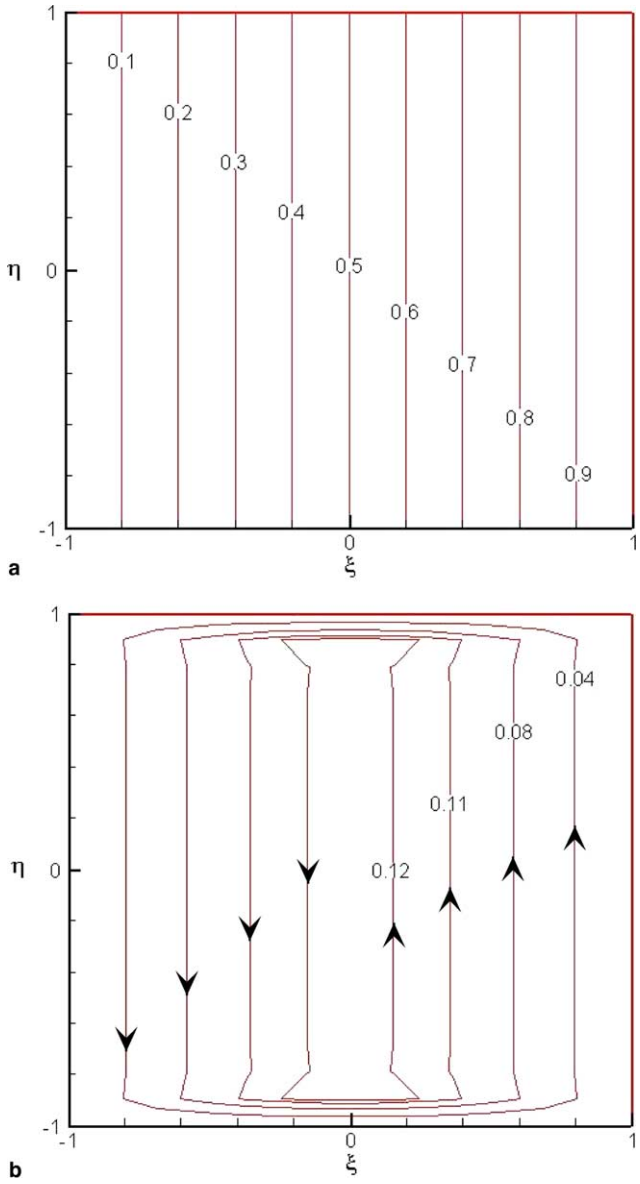

Fig. 3. Isotherms and streamlines in the melt for $B = 5$ T and $\alpha = 0.6$: (a) $T(\xi, \eta)$ and (b) $\psi(\xi, \eta)$.

circulation inside the parallel layer along $\eta = +1$. That is, along $\eta = +1$, $u = +0.07375$ at $\xi = 0$ and decreases to $u = 0$ as $|\xi|$ approaches ± 1. The interfacial shear stress of the slow-moving melt decreases the velocity of the encapsulant but does not drive flow in the opposite direction.

For $\alpha = 0.6$ and $B = 1$ T, the dimensionless parameters are $Ha = 1461.8$, $N = 4412.8$ and $Pe_t = 7.375$, and the characteristic velocity in the melt is $U = 0.0015706$ m/s. There is significantly less EM damping of the melt motion and the velocity of the melt is much larger. The maximum magnitude of the dimensional velocity in the melt and in the encapsulant are 0.005912 and 0.0000026158 m/s, respectively. The interfacial shear stress is much larger, as shown in Fig. 2, so

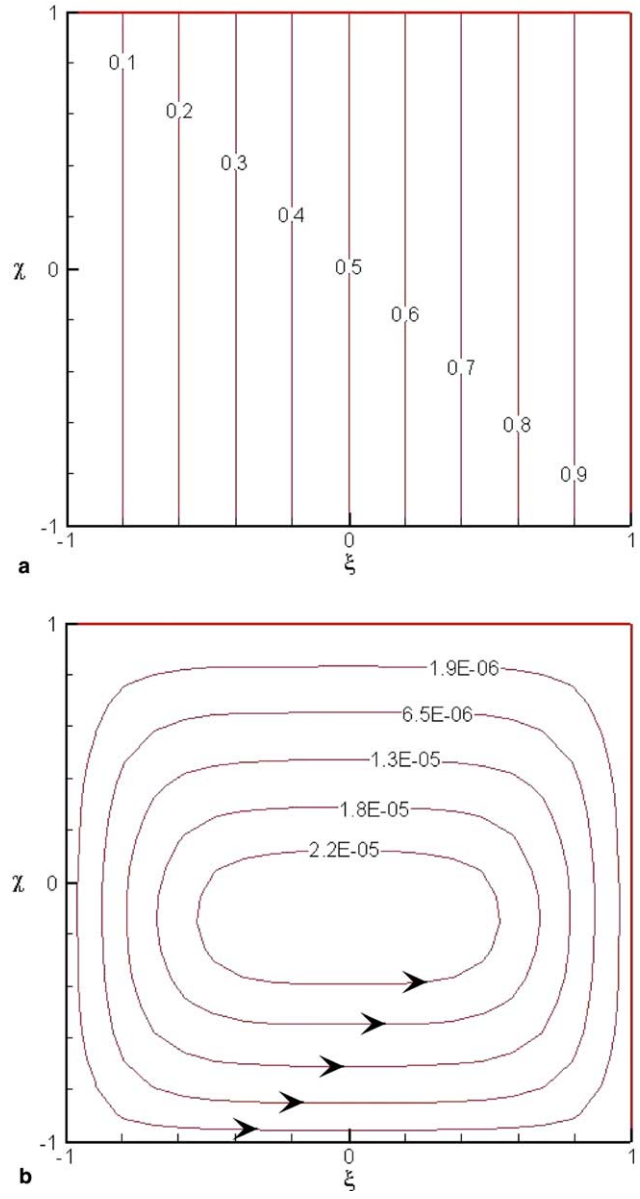

Fig. 4. Isotherms and streamlines in the encapsulant for $B = 5$ T and $\alpha = 0.6$: (a) $T_e(\xi, \chi)$ and (b) $\psi_e(\xi, \chi)$.

that the maximum value of the encapsulant's streamfunction is 0.000016398. We present the streamlines in the encapsulant in Fig. 5, in which the encapsulant's circulation is counterclockwise and the interfacial u is positive. In the melt, the maximum value of the streamfunction is 0.12979 with the bulk of the flow circulating in the counterclockwise direction. The natural convection in the encapsulant dominates and drives a positive interfacial velocity in the melt and a clockwise circulation inside the boundary layer along $\eta = +1$. That is, along $\eta = +1$, $u = +0.0006523$ at $\xi = 0$ and decreases to $u = 0$ as $|\xi|$ approaches ± 1. The interfacial shear stress of the slow-moving melt decreases the velocity of the encapsulant but does not drive flow in the opposite

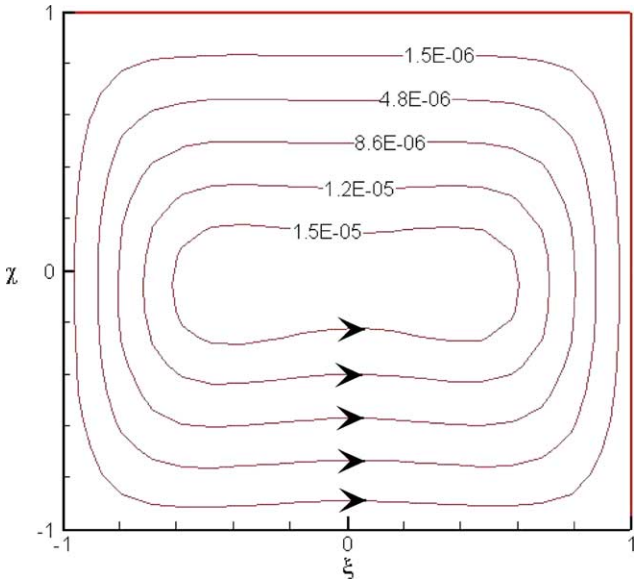

Fig. 5. Streamlines in the encapsulant $\psi_e(\xi, \chi)$ for $B = 1$ T and $\alpha = 0.6$.

direction. In both the melt and the encapsulant, the heat transfer remains dominated by conduction.

We further decrease the magnetic field strength to $B = 0.4$ T with $\alpha = 0.6$, the dimensionless parameters are $Ha = 584.7$, $N = 112.97$ and $Pe_t = 46.093$, and the characteristic velocity in the melt is $U = 0.009816$ m/s. In both the melt and the encapsulant, the heat transfer is still dominated by conduction. There is significantly less EM damping of the melt motion and the velocity of the melt is much larger as reflected in the maximum magnitude of the melt's dimensional velocity which is 0.02359 m/s. The maximum magnitude of the

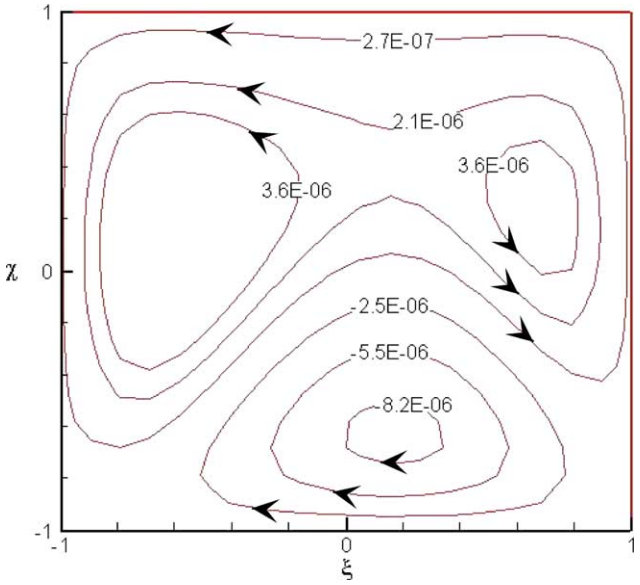

Fig. 6. Streamlines in the encapsulant $\psi_e(\xi, \chi)$ for $B = 0.4$ T and $\alpha = 0.6$.

encapsulant's dimensional velocity is 0.0000060506 m/s. In the melt, the maximum value of the streamfunction is 0.12935. The interfacial shear stress, which is presented in Fig. 2, is large enough to reverse some of the flow in the encapsulant as reflected in Fig. 6 where the minimum and maximum values of the streamfunction are −0.000008873 and 0.000007387, respectively. Along $\eta = +1$, $u = -0.0005834$ at $\xi = 0$ and increases to $u = 0$ as $|\xi|$ approaches ±1. As shown in Fig. 2, the maximum value of the interfacial shear stress is located at $\xi = 0.208$ and decreases as $|\xi|$ approaches ±1. The deviation from symmetry about $\xi = 0$ is reflected in the encapsulant's streamlines in Fig. 6.

4. Conclusions

The temperature gradient drives counterclockwise circulations in both the melt and encapsulant. These circulations alone would lead to positive and negative values of the horizontal velocity in the encapsulant and melt, respectively, near the interface. The competition between the two natural convections determines the direction of the horizontal velocity of the interface. For $\alpha = 0.6$ and $B = 5$ T, there is significant EM damping of the melt motion and the encapsulant drives a positive interfacial velocity and a small clockwise circulation in the melt. For $\alpha = 0.6$ and a much weaker field $B = 0.4$ T, the maximum velocity in the melt is thousands of times larger than that of the encapsulant, thus causing a large fraction of the encapsulant's volume to circulate in the clockwise direction.

Acknowledgement

This research was supported by the US Air Force Office of Scientific Research under grant FA9550-04-1-0249. The calculations were performed on the Cray X1 and the SGI Origin 3000 Complex provided by the DoD High Performance Computing Modernization Program under grant AFSNH2487 and on the IBM pSeries 690 provided by the National Computational Science Alliance under grant DMR030015.

References

Alchaar, S., Vasseur, P., Bilgen, E., 1995. Natural convection heat transfer in a rectangular enclosure with a transverse magnetic field. ASME Journal of Heat Transfer 117, 668–673.

Authie, G., Tagawa, T., Moreau, R., 2003. Buoyant flow in long vertical enclosures in the presence of a strong horizontal magnetic field. Part 2. Finite enclosures. European Journal of Mechanics B—Fluids 22, 203–220.

Burr, U., Müller, U., 2001. Rayleigh-Bénard convection in liquid metal layers under the influence of a vertical magnetic field. Physics of Fluids 13, 3247–3257.

Di Piazza, I., Ciofalo, M., 2002. MHD free convection in a liquid-metal filled cubic enclosure. I. Differential heating. International Journal of Heat and Mass Transfer 45, 1477–1492.

Farrell, M.V., Ma, N., 2002. Coupling of buoyant convections in boron oxide and a molten semiconductor in a vertical magnetic field. ASME Journal of Heat Transfer 124, 643–649.

Garandet, J.P., Alboussière, T., Moreau, R., 1992. Buoyancy driven convection in a rectangular enclosure with a transverse magnetic field. International Journal of Heat and Mass Transfer 35, 741–748.

Hirtz, J.M., Ma, N., 2000. Dopant transport during semiconductor crystal growth. Axial versus transverse magnetic fields. Journal of Crystal Growth 210, 554–572.

Hjellming, L.N., Walker, J.S., 1987. Melt motion in a Czochralski crystal puller with an axial magnetic field: motion due to buoyancy and thermocapillarity. Journal of Fluid Mechanics 182, 335–368.

Kuniholm, J.F., Ma, N., 2003. Natural convection in a liquid-encapsulated molten semiconductor with a steady magnetic field. International Journal of Heat and Fluid Flow 24, 130–136.

Ma, N., Walker, J.S., 1995. Liquid-metal buoyant convection in a vertical cylinder with a strong vertical magnetic field and with a nonaxisymmetric temperature. Physics of Fluids 7, 2061–2071.

Ma, N., Walker, J., Bliss, D., Bryant, G., 1998. Forced convection during liquid encapsulated crystal growth with an axial magnetic field. ASME Journal of Fluids Engineering 120, 844–850.

Ma, N., Walker, J.S., 2001. Inertia and thermal convection during crystal growth with a steady magnetic field. AIAA Journal of Thermophysics and Heat Transfer 15, 50–54.

Morton, J.L., Ma, N., Bliss, D.F., Bryant, G.G., 2002. Dopant segregation during liquid-encapsulated Czochralski crystal growth in a steady axial magnetic field. Journal of Crystal Growth 242, 471–485.

Mossner, R., Muller, U., 1999. A numerical investigation of three-dimensional magnetoconvection in rectangular cavities. International Journal of Heat and Mass Transfer 42, 1111–1121.

Ozoe, H., Okada, K., 1989. The effect of the direction of the external magnetic field on the three-dimensional natural convection in a cubical enclosure. International Journal of Heat and Mass Transfer 32, 1939–1954.

Riemann, H., Lüdge, A., Hallman, B., Turschner, T., 1996. Growth of floating zone (FZ) silicon crystals under the influence of a transversal magnetic field. In: Proceedings of the 4th International Symposium on High Purity Silicon, Electrochemical Society Proceedings 96-13, pp. 49–57.

Series, R.W., Hurle, D.T.J., 1991. The use of magnetic fields in semiconductor crystal growth. Journal of Crystal Growth 113, 305–328.

Walker, J.S., 1999. Models of melt motion, heat transfer and mass transport during crystal growth with strong magnetic fields. Progress in Crystal Growth and Characterization of Materials 38, 195–213.

Williams, M.G., Walker, J.S., 1990. Melt motion in a Czochralski puller with a weak transverse magnetic field. Journal of Crystal Growth 100, 233–253.